Gauge-invariant screening masses and static quark free energies in $N_f = 2 + 1$ QCD at nonzero baryon density

Michele Andreoli,[1,2,*] Claudio Bonati,[1,2,†] Massimo D'Elia,[1,2,‡] Michele Mesiti,[3,§] Francesco Negro,[2,‖] Andrea Rucci,[1,2,¶] and Francesco Sanfilippo[4,**]

[1]*Dipartimento di Fisica dell'Università di Pisa, Largo Pontecorvo 3, I-56127 Pisa, Italy*
[2]*INFN—Sezione di Pisa, Largo Pontecorvo 3, I-56127 Pisa, Italy*
[3]*Academy of advanced computing, Swansea University, Singleton Park, Swansea SA2 8PP, Wales, United Kingdom*
[4]*INFN—Sezione di Roma Tre, Via della Vasca Navale 84, I-00146 Roma, Italy*

(Received 9 January 2018; published 26 March 2018)

We discuss the extension of gauge-invariant electric and magnetic screening masses in the quark-gluon plasma to the case of a finite baryon density, defining them in terms of a matrix of Polyakov loop correlators. We present lattice results for $N_f = 2 + 1$ QCD with physical quark masses, obtained using the imaginary chemical potential approach, which indicate that the screening masses increase as a function of μ_B. A separate analysis is carried out for the theoretically interesting case $\mu_B/T = 3i\pi$, where charge conjugation is not explicitly broken and the usual definition of the screening masses can be used for temperatures below the Roberge-Weiss transition. Finally, we investigate the dependence of the static quark free energy on the baryon chemical potential, showing that it is a decreasing function of μ_B, which displays a peculiar behavior as the pseudocritical transition temperature at $\mu_B = 0$ is approached.

DOI: 10.1103/PhysRevD.97.054515

I. INTRODUCTION

Static color charges are useful probes of the properties of strongly interacting matter. At low temperature, the potential between a heavy quark-antiquark pair, which can be derived from Wilson loop expectation values or from Polyakov loop correlators, can be used to investigate the confining properties of the medium and the spectrum of heavy quark bound states. At high temperature, static charge interactions permit instead investigating screening effects in the quark-gluon plasma (QGP), which are at the basis of interesting phenomenology, like the dissociation of heavy quark bound states [1] (see Ref. [2] for a recent review). Moreover, the asymptotic (large-distance) behavior of Polyakov loop correlators gives access to the free energy of static color charges, which is a useful probe for confinement/deconfinement.

Interactions between heavy quarks have been widely studied in lattice QCD simulations by means of Polyakov loop correlators, in particular by projecting over color group representations (e.g., singlet or octet) after proper gauge fixing. Gauge-invariant observables can also be studied, and, using charge conjugation symmetry, it is possible to build gauge-invariant operators that couple only to the chromomagnetic or the chromoelectric sector [3,4]. In the high temperature phase, correlators of these observables permit defining in a gauge-invariant and nonperturbative way magnetic and electric screening masses (inverse of the screening lengths), which have been the subject of recent lattice QCD investigations [5,6].

Screening effects in the QGP are expected to be influenced by external parameters which can change the properties of the thermal medium. In general, an increase of color screening effects (i.e., an increase of the screening masses) is expected as the system is driven deeper into the deconfined region. An example is the introduction of a magnetic background field B, which is known to induce a decrease of the pseudocritical temperature T_c [7] and to affect the confining properties of QCD [8,9], favoring the onset of deconfinement. Magnetic and electric screening masses in the presence of an external background field have been determined by lattice simulations in Ref. [10] and have indeed been shown to be increasing functions of B,

*michele.andreoli@pi.infn.it
†claudio.bonati@df.unipi.it
‡massimo.delia@unipi.it
§michele.mesiti@swansea.ac.uk
‖fnegro@pi.infn.it
¶andrea.rucci@pi.infn.it
**francesco.sanfilippo@roma3.infn.it

in agreement with analytical studies of screening effects in the QGP [11–13].

The baryon chemical potential μ_B is another parameter of obvious phenomenological relevance. Also in this case, one expects an increase of screening effects as a function of μ_B, since a finite baryon density favors the onset of deconfinement; this is confirmed by perturbative predictions [14] and by lattice QCD studies considering correlators projected over color representations after gauge fixing [15]. In this case, however, when considering gauge-invariant screening masses, one has to face the problem that charge conjugation symmetry is explicitly broken by the presence of the baryon chemical potential, so a clear separation into electric and magnetic sectors cannot be performed anymore [4].

One of the purposes of this study is to propose an extension of the gauge-invariant definition of the screening masses to the case $\mu_B \neq 0$, which is based on the analysis of a full matrix of Polyakov loop correlators, i.e., including the mixed electric-magnetic correlator, which turns out to be nonzero when $\mu_B \neq 0$. Such an extension is then implemented in numerical simulations of $N_f = 2 + 1$ QCD with imaginary values of the baryon chemical potential, so the behavior of the gauge-invariant screening masses as a function of μ_B is finally obtained by analytic continuation to real μ_B. In this way, we will show that they increase as a function of μ_B. Special attention and a separate discussion will be devoted to those values of the imaginary chemical potential for which an exact charge conjugation symmetry can be recovered (Roberge-Weiss transition points).

A second aim of our study is the investigation of the dependence on μ_B of the free energy F_Q of a static color charge. This is related, after proper renormalization [6,16–19], to the large-distance behavior of Polyakov correlators and hence, by cluster property, to the Polyakov loop expectation value. This quantity has been extensively studied in the past, at finite T and zero chemical potential, for its connection to the confining properties of the thermal medium. Here, we consider the part of the free energy which is related to the introduction of the baryon chemical potential, $\Delta F_Q(T,\mu_B) \equiv F_Q(T,\mu_B) - F_Q(T,0)$ and can be obtained by studying the ratio of Polyakov loop expectation values. Also in this case, we will present numerical results obtained for imaginary values of μ_B and then exploit analytic continuation to extract the dependence of $\Delta F_Q(T,\mu_B)$ for small values of μ_B/T.

Simulations have been performed on a line of constant physics of $N_f = 2 + 1$ QCD with physical quark masses, discretized via stout improved staggered fermions. Most results have been obtained on a $32^3 \times 8$ lattice and for temperature above the pseudocritical temperature T_c. In particular, the screening masses have been investigated for temperatures ranging from 217 to 300 MeV, while a wider range has been explored to study the behavior of $\Delta F_Q(T,\mu_B)$. The paper is organized as follows. In Sec. II, we review the definition of the gauge-invariant screening masses in terms of Polyakov loop correlators and discuss the extension to the case of nonzero chemical potential. We then present the main features of the phase diagram at imaginary chemical potential, and we describe our numerical setup. In Sec. III, we present our results for the screening masses and the quark free energies as a function of μ_B. Finally, in Sec. IV, we draw our conclusions.

II. OBSERVABLES AND NUMERICAL METHODS

Our investigation is based on lattice QCD simulations. As is well known, the introduction of a baryon chemical potential μ_B makes the Euclidean path integral measure complex, so standard Monte-Carlo simulations are not feasible. A possible solution to this problem, which has been widely explored in the literature [20–43], is to perform simulations at imaginary values of the chemical potential, $\mu_B = i\mu_{B,I}$, then exploit analytic continuation, which is expected to be valid at least for sufficiently small values of μ_B/T.

We will consider a theory with $N_f = 2 + 1$ flavors (up, down, and strange) and physical quark masses. In order to move along a line of nonzero baryon chemical potential, with electric and strangeness chemical potentials set to zero, we have chosen degenerate quark chemical potentials $\mu_{f,I} = \mu_I \equiv \mu_{B,I}/3$. As usual, in the discretized theory, the chemical potentials are introduced in the Dirac operator in an exponentiated form attached to temporal gauge links [44], in order to avoid the insurgence of ultraviolet divergencies in the continuum limit. In this way, the introduction of a nonzero μ_B can also be viewed as a rotation of temporal boundary conditions for quark fields by a factor $\exp(\mu_B/(3T)) = \exp(i\mu_I/T)$.

A. Gauge-invariant screening masses at $\mu_B \neq 0$

It is well known that a perturbative definition of the screening masses of QCD [45–47] gets into trouble because of nonperturbative contributions arising in the finite temperature gluon propagator at the next-to–leading order, which are due to magnetostatic gluons and stem from the non-Abelian nature of the gauge group [48–51]. Nevertheless, it has been shown that well-defined screening masses can be accessed by studying the large-distance behavior of suitable correlators of gauge-invariant quantities, such as the Polyakov loops projected onto the electric and magnetic sectors [3,4]. In the continuum, the Polyakov loop is defined as

$$L(\mathbf{r}) = \frac{1}{N_c}\mathcal{P}\exp\left(ig\int_0^{1/T} d\tau A_0(\mathbf{r},\tau)\right), \qquad (1)$$

where $\mathcal{P}$ is the path-ordering operator and N_c is the number of colors; on the lattice, it is easily built in terms of gauge links in the temporal direction. As shown in Ref. [4]

(and retraced in some recent lattice works [5,6,10]), it is possible to separate the contributions to screening of the color-magnetic and color-electric gluons by defining suitable combinations of Polyakov loop correlators. This is achieved by performing a symmetry decomposition involving the Euclidean time reversal ($\mathcal{R}$) and the charge conjugation ($\mathcal{C}$) operators. As a result [4,6,10], one finds that the relevant role is played by the fluctuations of the real and imaginary parts of the Polyakov loop so that the correlators

$$C_{M^+}(\mathbf{r},T) = \langle \mathrm{TrRe}L(\mathbf{0})\mathrm{TrRe}L(\mathbf{r})\rangle - \langle \mathrm{TrRe}L\rangle^2,$$
$$C_{E^-}(\mathbf{r},T) = \langle \mathrm{TrIm}L(\mathbf{0})\mathrm{TrIm}L(\mathbf{r})\rangle - \langle \mathrm{TrIm}L\rangle^2 \qquad (2)$$

take contributions, respectively, only from the color-magnetic ($\mathcal{R}$-even and $\mathcal{C}$-even) and the color-electric ($\mathcal{R}$-odd and $\mathcal{C}$-odd) sectors. In the same way, it can be shown [6] that the cross sectors ($\mathcal{R}$-even and $\mathcal{C}$-odd or the opposite) are trivial; that manifests in the vanishing of the mixed correlators between the real and imaginary parts of the Polyakov loop. At large distances, these correlators are expected to behave as [3,4]

$$C_{M^+}(\mathbf{r},T)|_{r\to\infty} \simeq \frac{1}{r} e^{-m_M(T)r},$$
$$C_{E^-}(\mathbf{r},T)|_{r\to\infty} \simeq \frac{1}{r} e^{-m_E(T)r}, \qquad (3)$$

where $m_M(T)$ and $m_E(T)$ are the color-magnetic and color-electric screening masses.

The considerations above are valid when charge conjugation $\mathcal{C}$ is an exact symmetry of the theory. The introduction of a baryon chemical potential μ_B (or, in general, of chemical potentials coupled to quark number operators) breaks $\mathcal{C}$ explicitly, so a trivial extension of the definition of magnetic and electric screening masses to finite density QCD is not possible [4]. What happens is that the electric and the magnetic sectors are not separated anymore, a fact that manifests through the appearance of a nonzero mixed electric-magnetic correlator, which is defined as follows (we drop the dependence on T and μ_B for the sake of readability):

$$C_X(\mathbf{r}) = \langle \mathrm{TrRe}L(\mathbf{0})\mathrm{TrIm}L(\mathbf{r})\rangle - \langle \mathrm{TrRe}L\rangle\langle \mathrm{TrIm}L\rangle. \qquad (4)$$

A nonzero value of this correlator means that the real and the imaginary parts of the Polyakov loop do not undergo independent fluctuations anymore. The correlator is obviously symmetric under the exchange of electric and magnetic components, i.e., $\langle \mathrm{TrRe}L(\mathbf{0})\mathrm{TrIm}L(\mathbf{r})\rangle = \langle \mathrm{TrIm}L(\mathbf{0})\mathrm{TrRe}L(\mathbf{r})\rangle$ so that, when charge conjugation is explicitly broken, one can actually define a symmetric matrix of correlators:

$$\begin{pmatrix} C_{M^+}(\mathbf{r}) & C_X(\mathbf{r}) \\ C_X(\mathbf{r}) & C_{E^-}(\mathbf{r}) \end{pmatrix}. \qquad (5)$$

The practical effect of this mixing is that the asymptotic, large-distance behavior of all correlators will now be dominated by a single mass; that will be confirmed explicitly by our numerical data in the following. The information about the second gauge-invariant mass is now hidden in nonleading corrections to the asymptotic behavior of the correlators, which are usually difficult to detect directly.

This situation is quite common in the numerical investigation of the spectrum of quantum field theories, where one usually considers a set of mixed correlators in the same channel and needs to derive the masses of the lightest independent physical states coupled to them. A possible solution is to diagonalize the correlator matrix, i.e., to solve the eigenvalue equation

$$\mathbf{C}(\mathbf{r})\mathbf{x} = C_{1/2}(\mathbf{r})\mathbf{x}, \qquad (6)$$

where $\mathbf{C}$ stands for the matrix and the diagonal correlators C_1 and C_2 are easily found to be

$$C_{1/2}(\mathbf{r}) = \frac{1}{2}(C_{M^+}(\mathbf{r}) + C_{E^-}(\mathbf{r})) \pm \frac{1}{2}[(C_{M^+}(\mathbf{r}) - C_{E^-}(\mathbf{r}))^2 + 4C_X^2(\mathbf{r})]^{\frac{1}{2}}. \qquad (7)$$

Also, a straightforward computation leads to the following expression of the rotation angle,

$$\Theta(\mathbf{r}) = \frac{1}{2}\mathrm{atan}\left(\frac{2C_X(\mathbf{r})}{C_{M^+}(\mathbf{r}) - C_{E^-}(\mathbf{r})}\right), \qquad (8)$$

which takes a nonzero value when the mixing takes place. It is reasonable to expect the long-distance behavior of the diagonalized correlators to be similar to that found for the electric and magnetic ones at zero μ_B, i.e.,

$$C_{1/2}(\mathbf{r})|_{r\to\infty} \simeq \frac{1}{r} e^{-m_{1/2}r}, \qquad (9)$$

leading to the definition of two independent screening masses $m_1(T,\mu_B)$ and $m_2(T,\mu_B)$. Let us discuss the connection between this pair of states with those that can be determined at $\mu_B = 0$: if at $\mu_B = 0$ the excited state mass m_M^* in the magnetic sector is higher than m_E, these masses satisfy the natural relations $\lim_{\mu_B\to 0} m_1(T,\mu_B) = m_M(T)$ and $\lim_{\mu_B\to 0} m_2(T,\mu_B) = m_E(T)$. In general, it is not easy to extract the value of m_M^* with good precision; however, we have verified that in all the cases explored in this paper our numerical data are consistent with $m_M^*(\mu_B = 0) \geq m_E(\mu_B = 0)$.

Let us conclude with some remark on the variational approach used in the context of hadron spectroscopy

[52–54], which is different from the one described above. In that case, one solves a generalized eigenvalue problem

$$\mathbf{C}(\mathbf{r})\mathbf{x} = \lambda_{1/2}(\mathbf{r}, \mathbf{r}_0)\mathbf{C}(\mathbf{r}_0)\mathbf{x}, \tag{10}$$

where r_0 is a reference distance, which defines the so-called principal correlators $\lambda_{1/2}(\mathbf{r}, \mathbf{r}_0)$. We have verified that, in the explored cases, the two different approaches lead to consistent results. The results presented in the following will be based on the diagonal correlators $C_1(\mathbf{r})$ and $C_2(\mathbf{r})$.

B. The special case of the Roberge-Weiss point

As we have already mentioned above, the introduction of an imaginary baryon chemical potential can be rephrased in terms of a modification of the temporal boundary conditions for all quark fields by a phase $\theta = \mu_I/T$. That implies that an exact charge conjugation symmetry is recovered for special values of θ: $\theta = \pi$ is one example; however, all values $\theta = \pi(2k+1)/3$, with k integer, are equivalent to each other after a global center transformation on gauge fields [55]. In the case $\theta = \pi$, the charge conjugation symmetry has the same form as for $\mu_B = 0$, and it can also be viewed as a switch from thermal antiperiodic to periodic boundary conditions for fermion fields; therefore, we will take it as a reference in the following.

In this case, the standard definition of electric and magnetic screening masses could be maintained; however, it is well known that for such special values of θ charge conjugation undergoes a spontaneous breaking above some critical temperature [55], which is usually known as the Roberge-Weiss transition temperature T_{RW} and has been investigated in many lattice [56–67] and model [68–79] studies. For $T > T_{RW}$, the spontaneous breaking induces a mixed electric-magnetic correlator, so one needs to extend the definition of the gauge-invariant screening masses as discussed above.

On the contrary, for $T < T_{RW}$, one can keep the standard definition of electric and magnetic sectors and ask what modifications they undergo with respect to the standard case at zero chemical potential. In particular, one expects a significant change in the behavior of the electric correlator, since the imaginary part of the Polyakov loop is the order parameter of the Roberge-Weiss transition at $\theta = \pi$.

C. Dependence of the free energy on μ_B

The free energy F_Q of heavy quarks in the thermal medium can be inferred from the asymptotic behavior of the unsubtracted Polyakov loop correlator, i.e., the squared modulus of $\langle \mathrm{Tr}L \rangle$, as follows:

$$F_Q = -\frac{T}{2}\log|\langle \mathrm{Tr}L \rangle|^2. \tag{11}$$

This definition is plagued by additive ultraviolet divergencies and needs renormalization [6,16–19], which is usually performed by subtracting zero temperature contributions. However, the introduction of chemical potentials in the discretized theory is not expected to introduce further divergencies, at least when this is done by exponentiating it in the temporal gauge links [44], since that amounts to just a change of the temporal boundary conditions for fermion fields, which has no effect at all on the theory in the zero temperature limit (at least for small enough chemical potentials).

For this reason, the contribution to the heavy quark free energy related to the introduction of a baryon chemical potential,

$$\frac{\Delta F_Q(T,\mu_B,\beta)}{T} \equiv \frac{F_Q(T,\mu_B,\beta) - F_Q(T,0,\beta)}{T} = -\log\left(\frac{|\langle \mathrm{Tr}L \rangle(T,\mu_B,\beta)|}{|\langle \mathrm{Tr}L \rangle(T,0,\beta)|}\right), \tag{12}$$

where β is the inverse bare gauge coupling, is expected to be a renormalized quantity with a well-defined continuum limit. That will be checked explicitly, based on our numerical results, in Sec. III B.

D. Simulation details

We adopted a rooted staggered fermion discretization of $N_f = 2+1$ QCD. The partition function is

$$\mathcal{Z} = \int \mathcal{D}U e^{-\mathcal{S}_{\mathrm{YM}}} \prod_{f=u,d,s} \det\left[M^f_{\mathrm{st}}(U,\mu_{f,I})\right]^{1/4}, \tag{13}$$

where M^f_{st} and $\mu_{f,I}$ are, respectively, the fermion matrix and the imaginary chemical potential for the quark flavor f, while

$$\mathcal{S}_{\mathrm{YM}} = -\frac{\beta}{3}\sum_{i,\mu\neq\nu}\left(\frac{5}{6}W^{1\times1}_{i;\mu\nu} - \frac{1}{12}W^{1\times2}_{i;\mu\nu}\right) \tag{14}$$

is the tree level improved Symanzik gauge action [80,81] and $W^{n\times m}_{i;\mu\nu}$ stands for the trace of the $n\times m$ rectangular parallel transport starting from site i and spanning the μ-ν directions. The rooted staggered Dirac matrix

$$M^f_{\mathrm{st}}(U,\mu_{f,I}) = am_f\delta_{i,j} + \sum_{\nu=1}^{4}\frac{\eta_{i;\nu}}{2}\left[e^{ia\mu_{f,I}\delta_{\nu,4}}U^{(2)}_{i;\nu}\delta_{i,j-\hat{\nu}} - e^{-ia\mu_{f,I}\delta_{\nu,4}}U^{(2)\dagger}_{i-\hat{\nu};\nu}\delta_{i,j+\hat{\nu}}\right] \tag{15}$$

is written in terms of two times stout smeared links $U^{(2)}_{i;\nu}$ with isotropic smearing parameter $\rho = 0.15$ [82]. Bare parameters entering the action have been chosen so as to move on a line of constant physics [83–85], with degenerate light quark masses, $m_u = m_d = m_l$, a physical pion

TABLE I. Values of the bare coupling β we used for the determination of the screening masses, together with the corresponding lattice spacings a and temperatures T for our simulations on a $32^3 \times 8$ lattice. In each case, we report also the explored values of the imaginary quark chemical potential. The lattice spacing determination has a systematic uncertainty of the order of 2%–3% [84,85].

β	a(fm)	T(MeV)	$\mu_I/(\pi T)$
3.94	0.0821	300	0, 0.1, 0.2, 0.3, 1/3
3.8525	0.0984	251	0, 0.1, 0.2, 0.3, 1/3
3.8225	0.1052	234	0, 0.1, 0.2, 0.3, 1/3
3.79	0.1135	217	0, 0.1, 0.2, 0.3, 1/3

mass $m_\pi \simeq 135$ MeV, and a physical strange-to-light quark mass ratio $m_s/m_l = 28.15$.

Most of our Monte Carlo simulations have been performed for a fixed value of N_t, precisely on a $32^3 \times 8$ lattice. Screening masses have been measured for four values of the bare parameter β [corresponding to four different lattice spacings a and temperatures $T = 1/(aN_t)$] and various imaginary chemical potentials μ_I. The temperature range has been chosen in order to stay well above T_{RW}, which for $N_t = 8$ is $T_{RW} \simeq 200$ MeV [67], so that the full range of imaginary chemical potentials, up to the first Roberge-Weiss transition line at $\mu_I/T = \pi/3$, is available for analytic continuation. A summary of the simulation parameters is reported in Table I.

No attempt to estimate the magnitude of discretization effects is performed regarding the screening masses, since we have investigated just one lattice spacing for each temperature; however, we stress that results obtained at $\mu_B = 0$ [6] show that, in the same range of temperatures explored in our study, discretization errors for $N_t = 8$ lattices are not large and are within the statistical accuracy of the results that we are going to show.

Polyakov loop correlators have been measured, for each run, on a set of about 5×10^3 configurations separated by five molecular dynamics trajectories. For a noise-reduction technique, we have applied to temporal links three steps of APE smearing with parameter $\alpha = 0.5$. Correlators have been extracted for generic orientations (i.e., not just along the lattice axes) and distances using a Fast Fourier Transform algorithm, then averaging correlators corresponding to equal distances and different orientations. A blocked jackknife resampling technique has been used in order to correctly estimate statistical errors.

In order to extract the screening masses, a fit procedure based on the model in Eq. (3) has been performed, estimating the statistical errors on the mass parameters by resampling techniques. The errors reported in the following will also include systematic errors estimated by changing the range of fitted data points.

As for the determination of the static quark free energy $\Delta F_Q(T, \mu_B)$, given the better statistical accuracy which is reachable in this case even with limited statistics, we have explored a larger range of temperatures and also, in some cases, different values of N_t, in order to check for finite cutoff corrections. All numerical simulations have been performed using an Rational Hybrid Monte-Carlo (RHMC) algorithm running on Graphics Processing Units (GPUs) [86,87].

III. RESULTS

A. Screening masses

We start by discussing results obtained for Polyakov loop correlators and the gauge-invariant screening masses. In Fig. 1, we report some of the correlators obtained for lowest explored temperature, $T \simeq 217$ MeV. At zero chemical potential, the magnetic and electric correlators, C_{M^+} and C_{E^-}, show the standard behavior already clarified in previous studies [5,6,10]: the magnetic correlator is larger than the electric one, by around 1 order of magnitude, and decreases more slowly as a function of the distance, in agreement with the expected hierarchy $m_M < m_E$; best fits according to Eq. (3) are reported together with the data points. The mixed electric-magnetic correlator is zero

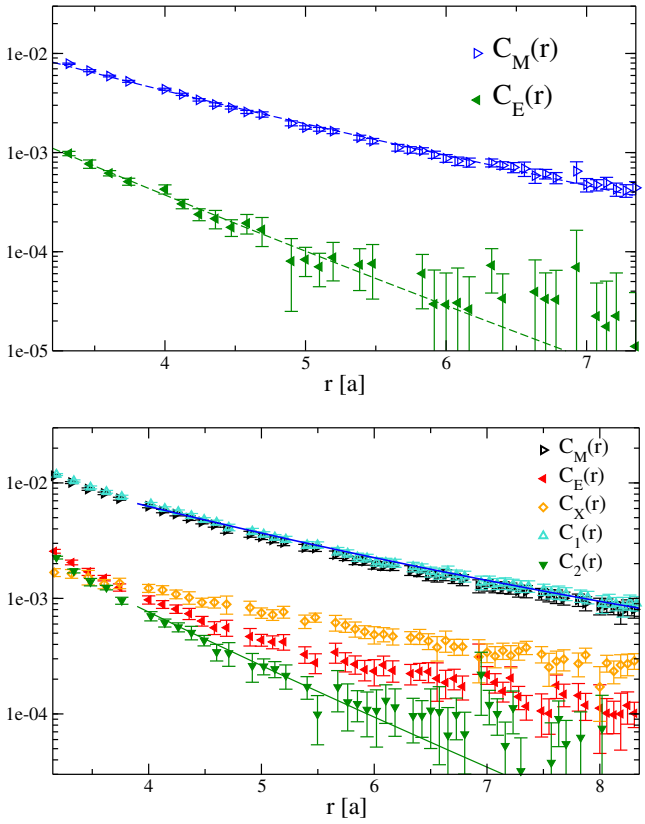

FIG. 1. Behavior of the color-magnetic C_M and color-electric C_E correlators at $T \simeq 217$ MeV and with $\mu_I/(\pi T) = 0$ (top) and $\mu_I/(\pi T) = 1/3$ (bottom). In this latter case, the mixed correlator C_X and the diagonalized correlators C_1 and C_2 are also shown for a comparison. Best fits to Eqs. (3) and (9) are shown, respectively, in the two cases.

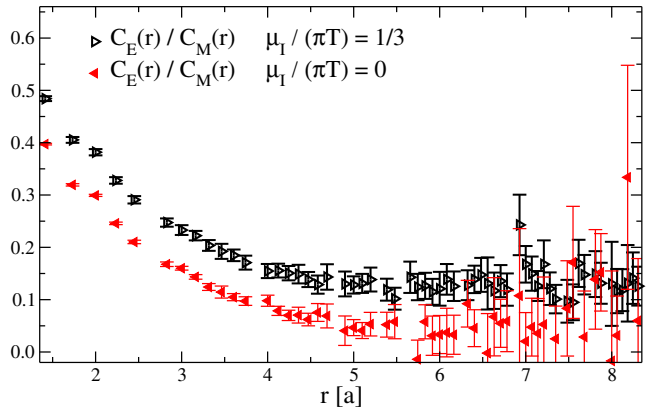

FIG. 2. Ratios between the electric and the magnetic correlator, as a function of the distance, for $T \simeq 217$ MeV, $\mu_I/(\pi T) = 1/3$ and $\mu_I/(\pi T) = 0$.

within statistical errors, as expected, and is not reported in the figure.

In Fig. 1, we report also correlators obtained at the same T for $\mu_I > 0$, in particular for $\mu_I/T = \pi/3$. In this case, the situation is quite different. The mixed correlator C_X turns out to be different from zero, and, as a result of this mixing, the long-range behavior of the electric correlator is modified; indeed, apart from an overall factor, the magnetic and the electric correlators show the same behavior at large distances, which seems to be governed by the same long-distance correlations length. This phenomenon is more clearly visible in Fig. 2, where the ratio C_{E^-}/C_{M^+} is reported as a function of r: while at $\mu_I = 0$, the ratio becomes compatible with zero at large distances, and at $\mu_I \neq 0$, it approaches a constant nonzero value, which indicates that the two correlators fall off in the same way and that their large-distance behavior is dominated by one single mass.

This mixing is eliminated when one considers the two diagonalized correlators C_1 and C_2 defined in Eq. (7), which permits obtaining two well-distinct screening masses m_1 and m_2. An example of such correlators is shown in Fig. 1, together with a best fit according to Eq. (9). The whole set of diagonalized correlators at $T \simeq 217$ MeV is shown in Fig. 3, for all the explored values of the imaginary chemical potential.

It is also interesting to consider the behavior of the mixing angle $\Theta(r)$, defined in Eq. (8), which is reported in Fig. 4 as a function of r for different values of the chemical potential. $\Theta(r)$ increases both as a function of the distance r and of the chemical potential; moreover, it seems to reach a plateau for large separations between the Polyakov loops at fixed μ_I/T. While a precise determination of these asymptotic values would require higher statistics and it is beyond the scope of the present work, their approximate values are reported in Fig. 5 as a function of the chemical potential for different temperatures: at fixed μ_I/T, the asymptotic mixing angle decreases as a function of temperature, which is

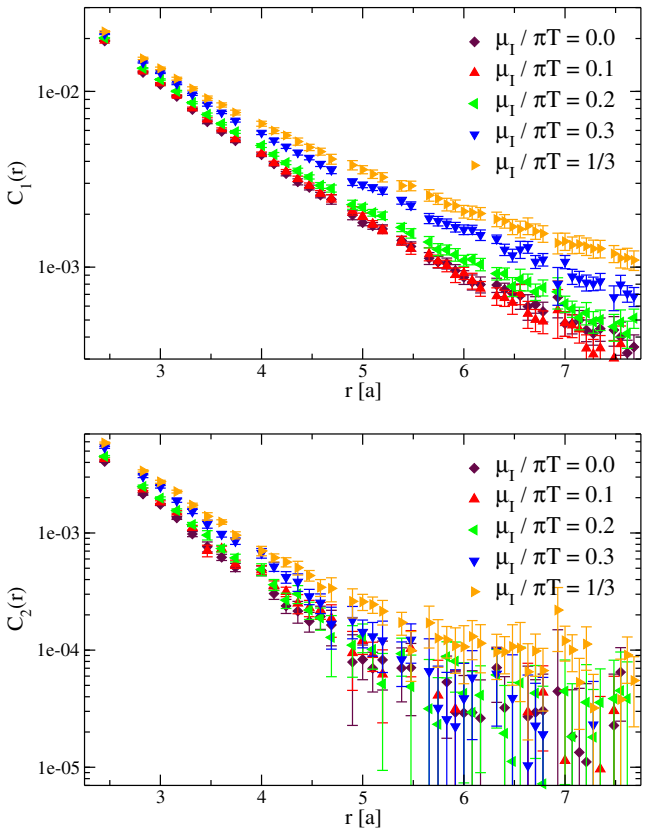

FIG. 3. Behavior of the diagonalized correlators C_1 and C_2 at $T \simeq 217$ MeV for different values of the imaginary chemical potential.

likely due to the fact that the effective potential of the Polyakov loop makes it stiffer at high temperatures. We note that the fit ranges used to extract the screening masses correspond roughly to the regions in which $\Theta(r)$ seems to reach the plateaux.

The gauge-invariant screening masses that we have obtained are reported as a function of $\mu_I/(\pi T)$ and for

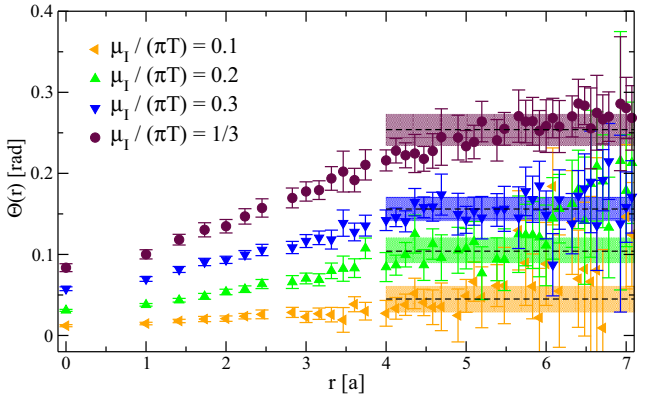

FIG. 4. Dependence of the mixing angle on the distance between the Polyakov loops at $T \simeq 217$ MeV for different values of the imaginary chemical potential. The estimated asymptotic values of $\Theta(r)$ are represented by the horizontal bands.

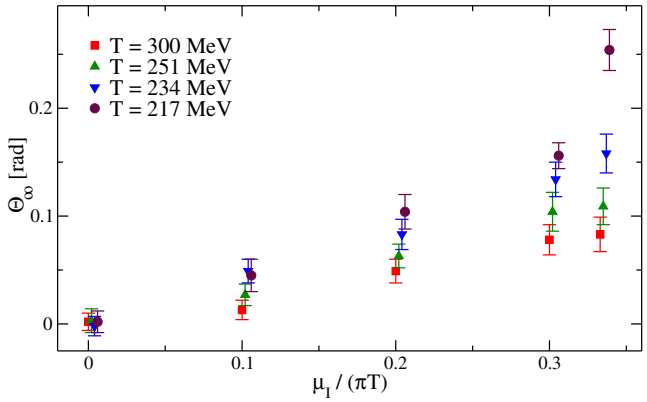

FIG. 5. Plateau values of the mixing angle as a function of the imaginary chemical potential for different values of the temperature. Data have been slightly shifted horizontally to improve the readability.

various temperatures in Table II and plotted in Fig. 6. Actually, we report the quantity $m_{1/2}/T$, since this dimensionless ratio is known to be almost independent of T at zero chemical potential. Reported error bars include also systematic errors related to the choice of fitting range.

The screening masses are expected to be even functions of μ_B. Therefore, at the leading order in a Taylor expansion, we can write the following general ansatz,

$$\frac{m_{1/2}(\mu_B, T)}{T} = a_{1/2}(T)\left[1 + b_{1/2}(T)\left(\frac{\mu_B}{3\pi T}\right)^2\right], \qquad (16)$$

TABLE II. Screening masses obtained for the explored values of T and $\mu_I/(\pi T)$.

T (MeV)	$\mu_I/\pi T$	m_1/T	m_2/T
217	0.0	3.57(50)	9.2(1.4)
	0.1	4.28(57)	9.8(1.2)
	0.2	3.28(46)	8.6(1.6)
	0.3	2.98(48)	9.4(1.1)
	1/3	1.97(35)	7.0(1.4)
234	0.0	4.18(43)	9.2(1.5)
	0.1	4.67(59)	8.9(1.3)
	0.2	3.71(42)	8.5(1.2)
	0.3	3.74(36)	10.4(1.0)
	1/3	2.05(35)	9.1(0.9)
251	0.0	4.81(33)	10.9(1.0)
	0.1	5.06(34)	9.1(1.2)
	0.2	4.44(29)	8.8(1.1)
	0.3	3.89(30)	8.7(0.9)
	1/3	4.00(31)	8.3(1.0)
300	0.0	4.90(36)	8.2(1.6)
	0.1	5.10(38)	9.9(1.0)
	0.2	5.06(33)	9.3(0.9)
	0.3	4.25(31)	9.7(1.1)
	1/3	3.46(43)	7.2(1.1)

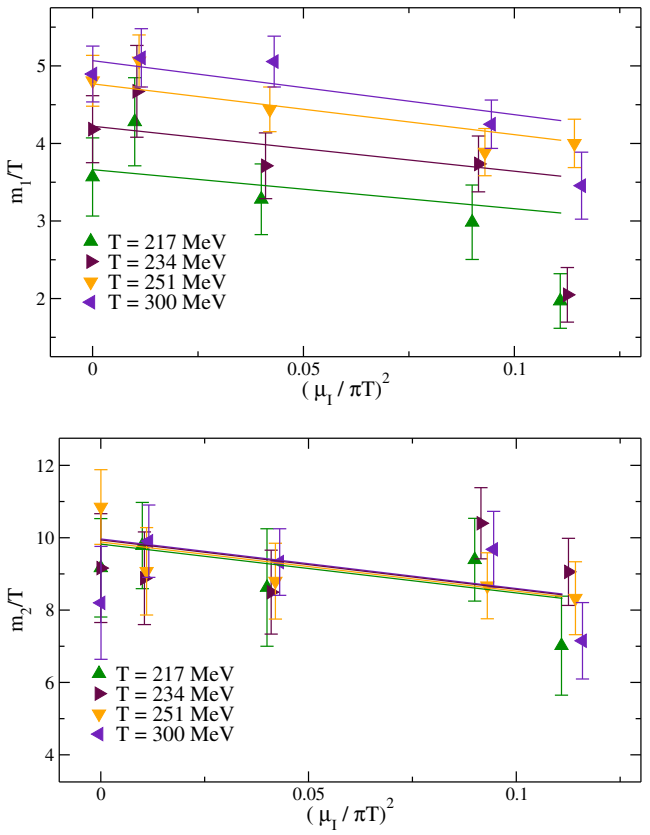

FIG. 6. Diagonalized masses m_1/T and m_2/T as function of $\mu_I/(\pi T)$ for different temperatures. Curves are the result of a best fit using the ansatz in Eq. (16) and setting $b_{1/2}(T) = b$ where b is a constant (see the text).

where $\mu_B = 3i\mu_I$. In our fit, we have discarded the values obtained for $\mu_I/(\pi T) = 1/3$, the reason being that for this value of the chemical potential the screening masses are expected to vanish with a nonanalytical behavior as the temperature approaches the second order Roberge-Weiss endpoint from above [67].

As a matter of fact, it is possible to fit all data using a unique value for the quadratic coefficients, i.e., setting $b_{1/2}(T) = b$, where b is a T independent constant, obtaining $b = 1.37(36)$ with $\chi^2 = 15.24/23$. A positive value b indicates that screening masses increase as a function of μ_B; this is in qualitative agreement with the fact that the introduction of a finite baryon density tends to drive the system farther away from the confined phase. The fact that b is independent of T is in agreement with leading order perturbative estimates of the Debye screening mass [14] giving $b = 1.5N_f/(6 + N_f) = 0.5$ for $N_f = 3$, which is not far from our estimate. The fact that a common value of b describes both masses implies that the ratio m_1/m_2 is independent of μ_B; notice, however, that our data do not put a stringent constraint on this and there is room for different behaviors within the present errors.

B. Results on the dependence of the quark free energy on μ_B

Let us turn to a discussion of the results obtained for the dependence of the heavy quark free energy on the baryon chemical potential, $\Delta F_Q(\mu_B, T)$, defined in Eq. (12). To start with, we show in Fig. 7 the results obtained at $T \simeq 251$ MeV for two different values of the temporal extension, $N_t = 6$, 8, and from both smeared and unsmeared Polyakov loops. The fact that all determinations agree within errors is a convincing test that this quantity is well defined and does not need renormalization, as expected. Moreover, data suggest that $O(a^2)$ corrections are not significant, within present errors, already for $N_t = 6$.

It is not the aim of this study to provide a continuum extrapolation for $\Delta F_Q(\mu_B, T)$; therefore, for the other temperatures, we just provide results obtained for $N_t = 8$, which are shown for some of the explored temperatures in Fig. 8. The free energy is expected to be an even and analytic function of the chemical potential; therefore, fitting numerical data with a truncated Taylor expansion in $(\mu_B/T)^2$ is the natural choice. Within the statistical accuracy of our data,

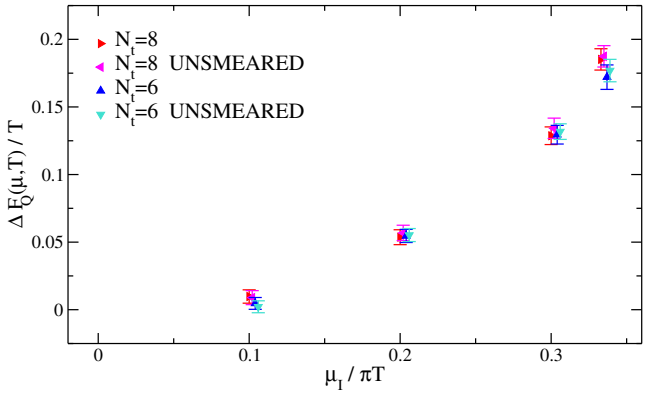

FIG. 7. $\Delta F_Q(\mu_B, T)/T$ at $T = 251$ MeV, obtained from the ratio of Polyakov loops with and without smearing and for two different values of N_t.

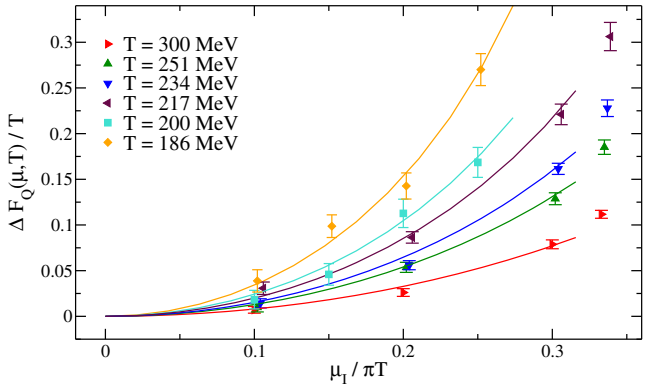

FIG. 8. $\Delta F_Q(\mu_B, T)/T$ at various temperatures obtained from the ratios of smeared Polyakov loops on lattices with $N_t = 8$.

TABLE III. Results for the coefficient χ_{Q,μ_B^2} entering the parametrization of $\Delta F_Q(\mu_B, T)$ defined in Eq. (17), as obtained from a fit to our numerical data for $\mu_I/T < \pi/3$.

T	χ_{Q,μ_B^2}	χ^2/dof
185	0.0742(33)	3.52/3
200	0.0530(32)	1.64/3
217	0.0440(17)	2.78/2
234	0.0341(10)	3.96/2
251	0.0288(11)	0.56/2
300	0.0179(9)	3.68/2

we are able to reliably estimate just the first term in the expansion; moreover, we have noticed that the quality of the fit improves if one tries to fit directly the behavior of the squared ratio of Polyakov loops, i.e., the exponential of the free energy, according to

$$\frac{|\langle \mathrm{Tr}L\rangle(T,\mu_B)|^2}{|\langle \mathrm{Tr}L\rangle(T,0)|^2} = \exp\left(-2\frac{\Delta F_Q(\mu_B,T)}{T}\right) = 1 - \chi_{Q,\mu_B^2}\left(\frac{\mu_B}{T}\right)^2 + O((\mu_B/T)^4), \quad (17)$$

where

$$\chi_{Q,\mu_B^2} \equiv \frac{\partial^2(F_Q/T)}{\partial(\mu_B/T)^2}. \quad (18)$$

Such a functional dependence, with higher order terms neglected, describes reasonably well data with $\mu_I/T < \pi/3$ at all temperatures; the results of our best fits are reported in Table III.

The analytic continuation of $\Delta F_Q(\mu_B, T)$ to real chemical potentials according to Eq. (17) is shown in Fig. 9. The free energy of the static quark is a decreasing function of μ_B, in agreement with the fact that a finite baryon chemical potential enhances deconfinement. Also, the fact that the

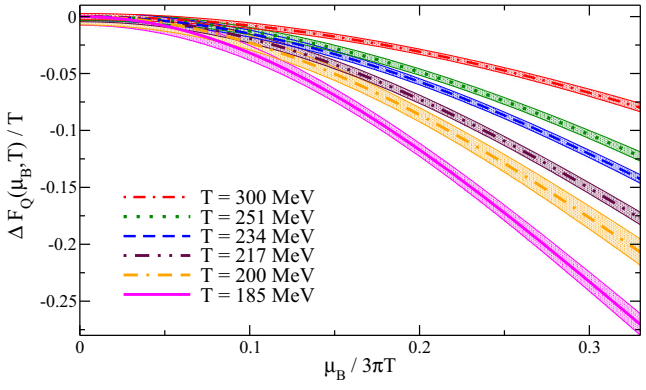

FIG. 9. Analytic continuation of $\Delta F_Q(\mu_B, T)/T$ to real chemical potentials, obtained from a best fit to our numerical data at imaginary chemical potential and assuming the ansatz in Eq. (17).

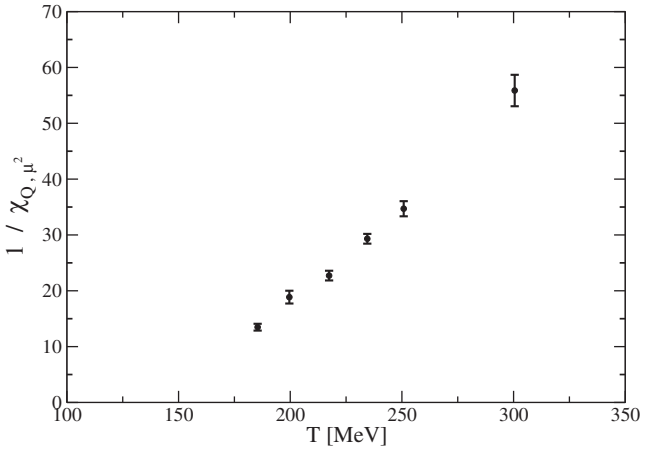

FIG. 10. Behavior of the inverse of the coefficient χ_{Q,μ_B^2}, defined in Eq. (17), as a function of temperature.

coefficient χ_{Q,μ_B^2} becomes larger as T decreases can be understood qualitatively. Close to the pseudocritical temperature, the chemical potential acts as a transition driving parameter; if the Polyakov loop were an exact order parameter for deconfinement, its dependence on μ_B would become sharper and eventually diverge at the transition. Of course this is not the case. The Polyakov loop is not an order parameter, and there is no real transition in QCD at the physical point; however, it is reasonable to expect χ_{Q,μ_B^2} to become larger and larger as T_c is approached from above.

This behavior is clearly visible in Fig. 10, where we plot the inverse coefficient, $1/\chi_{Q,\mu_B^2}$ as a function of T. It is striking to notice that, looking at the high temperature region, one would be tempted to predict a vanishing of $1/\chi_{Q,\mu_B^2}$ in a region of temperatures around 150 MeV, i.e., roughly coinciding with T_c. Of course, the behavior is then smoothed out as T_c is approached more closely. We cannot assert if this hints at a more strict connection between $\Delta F_Q(\mu_B, T)$ and the confinement/deconfinement transition; however, it indicates that this is a quantity which is surely worth further investigation.

C. Magnetic and electric screening masses close to the Roberge-Weiss endpoint

As we have stressed above, values of the imaginary chemical potential which at high T lead to the Roberge-Weiss transition play a special role. Consider in particular the case $\mu_I/T = \pi$, which corresponds to a simple shift of fermionic boundary conditions from antiperiodic to periodic ones; charge conjugation symmetry is not explicitly broken in this case. For $T > T_{RW}$, it gets spontaneously broken, so a mixing between the electric and the magnetic sectors appears anyway; however. for $T < T_{RW}$, it is not, and the standard definition of electric and magnetic correlators, with the associated screening masses, is well posed, so it is interesting to compare their behavior with the case of zero chemical potential.

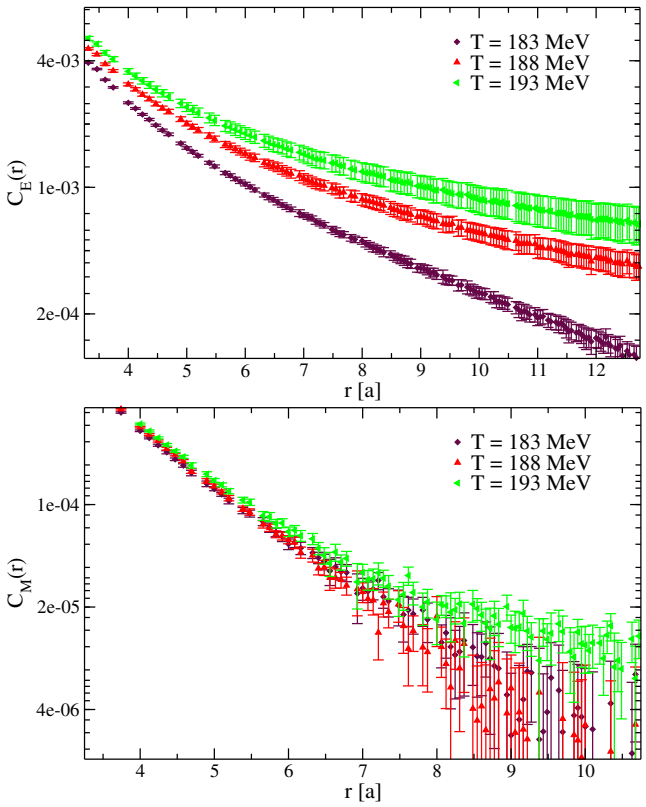

FIG. 11. Behavior of the color-electric (top) and color-magnetic (bottom) correlators measured on a $40^3 \times 8$ lattice at $\mu_I/T = \pi$ and for three different temperatures below $T_{RW}(N_t = 8) \sim 200$ MeV.

In Fig. 11, we show the behavior of such correlators for three values of T. A striking difference with respect to the $\mu_I/T = 0$ case is clearly visible: the hierarchy is inverted, with the electric correlators being larger than the magnetic ones by more than 1 order of magnitude and growing significantly as T approaches T_{RW}, which for the $40^3 \times 8$ lattice that we have used for these measurements is $T_{RW}(N_t = 8) \sim 200$ MeV [67].

The reason is easy to understand: the electric correlator is the two-point function of the imaginary part of the Polyakov loop [see Eq. (2)], which is also an order parameter for the Roberge-Weiss transition at $\mu_I/T = \pi$. Therefore, being directly connected to the order parameter of the transition, it is expected to undergo the most critical modifications, due to large-distance fluctuations, as one approaches the critical point.

To better clarify this point, we show the values of the electric screening masses at $\mu_I/T = \pi$ [defined as in Eq. (3)] as a function of T in Fig. 12. The electric mass decreases rapidly as T approaches T_{RW}, seemingly approaching zero at the transition, as expected. Notice, however, that, within the present statistical errors and limited number of data points, we are not able to check whether we are already close enough to T_{RW} to reveal the correct critical behavior predicted for the correlation length at the transition, which for this case is in the three-dimensional Ising universality class [67].

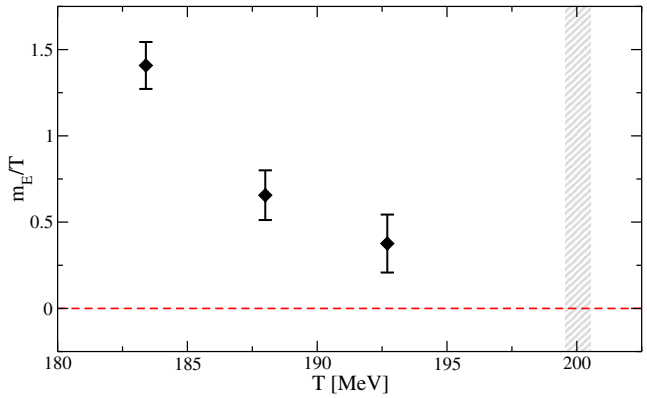

FIG. 12. Electric screening masses at $\mu_I/T = \pi$ obtained from the correlators shown in Fig. 11. The vertical gray band indicates the location of T_{RW} for $N_t = 8$ [67]; notice that in this case we report just the statistical error stemming from the determination of the critical coupling in Ref. [67] and not the systematic one stemming from the determination of the overall physical scale, which is common to all data in this limited range of temperatures.

IV. CONCLUSIONS

We have investigated the behavior of Polyakov loops and of Polyakov loop correlators as a function of the baryon chemical potential in the deconfined phase of QCD with $N_f = 2 + 1$ flavors and physical quark masses.

We have discussed the extension of the concept of gauge-invariant screening masses at finite baryon density, where charge conjugation symmetry is explicitly broken and a mixing between the electric and the magnetic sector appears, leading to the inapplicability of the standard definition of color-electric and color-magnetic masses. Such an extension can be given in terms of diagonalized (or alternatively principal) correlators derived from a 2×2 matrix of correlators involving the real and the imaginary parts of the Polyakov loop. In this way, one can obtain a consistent definition of two different gauge-invariant screening masses which characterize the thermal medium in the presence of a finite baryon density.

In order to obtain a determination of such screening masses, we have considered the theory discretized on $N_t = 8$ lattices by means of stout smeared rooted staggered fermions and a tree level Symanzik improved gauge action. Numerical simulations have been performed using imaginary values of the baryon chemical potential, then exploiting analytic continuation. Both screening masses show an increasing behavior as the baryon chemical potential is switched on, and the slope of the relative increase [see Eq. (16)] seems to be independent of T and of the same order of magnitude as that predicted for the Debye screening mass at the lowest order of perturbation theory. Future investigations should extend present results to different values of N_t in order to provide a continuum extrapolation for the gauge-invariant screening masses at finite baryon density.

We have also shown that for $\mu_I/T = \pi$ and $T < T_{RW}$, where charge conjugation symmetry is exact and the standard definitions of electric and magnetic screening masses still holds, the hierarchy of screening lengths is inverted, with the electric mass being the lowest one and approaching zero as $T \to T_{RW}$. This has been interpreted in terms of the direct coupling existing between the electric correlator and the order parameter for the Roberge-Weiss transition.

Finally, we have investigated the dependence of the static quark free energy on the chemical potential, which is defined by the large-distance behavior of the Polyakov loop correlators. In particular, we have considered the free energy variation due to the introduction of the chemical potential, $\Delta F_Q(\mu_B, T)$, which is related to the ratio of Polyakov loops and is not expected to undergo additive renormalization; this has been explicitly verified by comparing data obtained for different values of N_t and different amounts of smearing on Polyakov loops. The static free energy decreases as a function of the baryon chemical potential, as expected on general grounds, with a slope which increases significantly as the temperature approaches the pseudocritical temperature T_c from above. That could hint at a more strict connection between $\Delta F_Q(\mu_B, T)$ and the confinement/deconfinement transition; future investigations should consider a more systematic study of this quantity and its extrapolation to the continuum limit.

ACKNOWLEDGMENTS

We thank A. Bazavov for useful discussions. Numerical simulations have been performed on the GALILEO machine at CINECA, based on the agreement between INFN and CINECA (under Project No. INF17_npqcd) and at the Scientific Computing Center at INFN-PISA. F. N. acknowledges financial support from the INFN HPC_HTC project.

[1] T. Matsui and H. Satz, Phys. Lett. B **178**, 416 (1986).
[2] A. Andronic *et al.*, Eur. Phys. J. C **76**, 107 (2016).
[3] E. Braaten and A. Nieto, Phys. Rev. Lett. **74**, 3530 (1995).
[4] P. B. Arnold and L. G. Yaffe, Phys. Rev. D **52**, 7208 (1995).
[5] Y. Maezawa, S. Aoki, S. Ejiri, T. Hatsuda, N. Ishii, K. Kanaya, N. Ukita, and T. Umeda (WHOT-QCD Collaboration), Phys. Rev. D **81**, 091501 (2010).

[6] S. Borsányi, Z. Fodor, S. D. Katz, A. Pásztor, K. K. Szabó, and C. Török, J. High Energy Phys. 04 (2015) 138.
[7] G. S. Bali, F. Bruckmann, G. Endrodi, Z. Fodor, S. D. Katz, S. Krieg, A. Schafer, and K. K. Szabo, J. High Energy Phys. 02 (2012) 044.
[8] C. Bonati, M. D'Elia, M. Mariti, M. Mesiti, F. Negro, and F. Sanfilippo, Phys. Rev. D **89**, 114502 (2014).
[9] C. Bonati, M. D'Elia, M. Mariti, M. Mesiti, F. Negro, A. Rucci, and F. Sanfilippo, Phys. Rev. D **94**, 094007 (2016).
[10] C. Bonati, M. D'Elia, M. Mariti, M. Mesiti, F. Negro, A. Rucci, and F. Sanfilippo, Phys. Rev. D **95**, 074515 (2017).
[11] A. Bandyopadhyay, C. A. Islam, and M. G. Mustafa, Phys. Rev. D **94**, 114034 (2016).
[12] M. Hasan, B. Chatterjee, and B. K. Patra, Eur. Phys. J. C **77**, 767 (2017).
[13] B. Singh, L. Thakur, and H. Mishra, arXiv:1711.03071.
[14] M. Le Bellac, *Thermal Field Theory* (Cambridge University Press, Cambridge, England, 1996).
[15] J. Takahashi, K. Nagata, T. Saito, A. Nakamura, T. Sasaki, H. Kouno, and M. Yahiro, Phys. Rev. D **88**, 114504 (2013); *Proc. Sci.*, LATTICE2013 (2014) 166.
[16] O. Kaczmarek, F. Karsch, P. Petreczky, and F. Zantow, Phys. Lett. B **543**, 41 (2002).
[17] P. Petreczky and K. Petrov, Phys. Rev. D **70**, 054503 (2004).
[18] O. Kaczmarek, *Proc. Sci.*, CPOD07 (2007) 043.
[19] O. Kaczmarek and F. Zantow, arXiv:hep-lat/0506019.
[20] M. G. Alford, A. Kapustin, and F. Wilczek, Phys. Rev. D **59**, 054502 (1999).
[21] M.-P. Lombardo, Nucl. Phys. B, Proc. Suppl. **83**, 375 (2000).
[22] P. de Forcrand and O. Philipsen, Nucl. Phys. **B642**, 290 (2002); **B673**, 170 (2003); J. High Energy Phys. 01 (2007) 077; 11 (2008) 012.
[23] M. D'Elia and M. P. Lombardo, Phys. Rev. D **67**, 014505 (2003); **70**, 074509 (2004).
[24] V. Azcoiti, G. Di Carlo, A. Galante, and V. Laliena, Nucl. Phys. **B723**, 77 (2005).
[25] H. S. Chen and X. Q. Luo, Phys. Rev. D **72**, 034504 (2005).
[26] F. Karbstein and M. Thies, Phys. Rev. D **75**, 025003 (2007).
[27] P. Cea, L. Cosmai, M. D'Elia, and A. Papa, J. High Energy Phys. 02 (2007) 066; Phys. Rev. D **77**, 051501 (2008); **81**, 094502 (2010).
[28] L. K. Wu, X. Q. Luo, and H. S. Chen, Phys. Rev. D **76**, 034505 (2007).
[29] K. Nagata and A. Nakamura, Phys. Rev. D **83**, 114507 (2011).
[30] P. Giudice and A. Papa, Phys. Rev. D **69**, 094509 (2004).
[31] M. D'Elia, F. Di Renzo, and M. P. Lombardo, Phys. Rev. D **76**, 114509 (2007).
[32] P. Cea, L. Cosmai, M. D'Elia, C. Manneschi, and A. Papa, Phys. Rev. D **80**, 034501 (2009).
[33] A. Alexandru and A. Li, *Proc. Sci.*, LATTICE2013 (2013) 208.
[34] P. Cea, L. Cosmai, M. D'Elia, A. Papa, and F. Sanfilippo, Phys. Rev. D **85**, 094512 (2012).
[35] M. D'Elia and F. Sanfilippo, Phys. Rev. D **80**, 014502 (2009).
[36] T. Takaishi, P. de Forcrand, and A. Nakamura, *Proc. Sci.*, LAT2009 (2009) 198.
[37] P. Cea, L. Cosmai, and A. Papa, Phys. Rev. D **89**, 074512 (2014); **93**, 014507 (2016).
[38] C. Bonati, P. de Forcrand, M. D'Elia, O. Philipsen, and F. Sanfilippo, Phys. Rev. D **90**, 074030 (2014).
[39] C. Bonati, M. D'Elia, M. Mariti, M. Mesiti, F. Negro, and F. Sanfilippo, Phys. Rev. D **90**, 114025 (2014); **92**, 054503 (2015).
[40] R. Bellwied, S. Borsanyi, Z. Fodor, J. Gunther, S. D. Katz, C. Ratti, and K. K. Szabo, Phys. Lett. B **751**, 559 (2015).
[41] J. Gunther, R. Bellwied, S. Borsanyi, Z. Fodor, S. D. Katz, A. Pasztor, and C. Ratti, Eur. Phys. J. Web Conf. **137**, 07008 (2017).
[42] M. D'Elia, G. Gagliardi, and F. Sanfilippo, Phys. Rev. D **95**, 094503 (2017).
[43] V. G. Bornyakov *et al.*, arXiv:1712.02830.
[44] P. Hasenfratz and F. Karsch, Phys. Lett. **125B**, 308 (1983).
[45] D. J. Gross, R. D. Pisarski, and L. G. Yaffe, Rev. Mod. Phys. **53**, 43 (1981).
[46] J. I. Kapusta and C. Gale, *Finite-Temperature Field Theory. Principles and Applications* (Cambridge University Press, Cambridge, England, 2006).
[47] M. Laine and A. Vuorinen, Lect. Notes Phys. **925**, 1 (2016).
[48] S. Nadkarni, Phys. Rev. D **33**, 3738 (1986).
[49] A. K. Rebhan, Phys. Rev. D **48**, R3967 (1993).
[50] A. K. Rebhan, Nucl. Phys. **B430**, 319 (1994).
[51] E. Braaten and A. Nieto, Phys. Rev. Lett. **73**, 2402 (1994).
[52] C. Michael, Nucl. Phys. **B259**, 58 (1985).
[53] M. Luscher and U. Wolff, Nucl. Phys. **B339**, 222 (1990).
[54] B. Blossier, M. Della Morte, G. von Hippel, T. Mendes, and R. Sommer, J. High Energy Phys. 04 (2009) 094.
[55] A. Roberge and N. Weiss, Nucl. Phys. **B275**, 734 (1986).
[56] T. DeGrand and R. Hoffmann, J. High Energy Phys. 02 (2007) 022.
[57] B. Lucini, A. Patella, and C. Pica, Phys. Rev. D **75**, 121701 (2007).
[58] M. D'Elia and F. Sanfilippo, Phys. Rev. D **80**, 111501 (2009).
[59] P. de Forcrand and O. Philipsen, Phys. Rev. Lett. **105**, 152001 (2010).
[60] C. Bonati, G. Cossu, M. D'Elia, and F. Sanfilippo, Phys. Rev. D **83**, 054505 (2011).
[61] O. Philipsen and C. Pinke, Phys. Rev. D **89**, 094504 (2014).
[62] L.-K. Wu and X.-F. Meng, Phys. Rev. D **87**, 094508 (2013); **90**, 094506 (2014).
[63] K. Nagata, K. Kashiwa, A. Nakamura, and S. M. Nishigaki, Phys. Rev. D **91**, 094507 (2015).
[64] T. Makiyama, Y. Sakai, T. Saito, M. Ishii, J. Takahashi, K. Kashiwa, H. Kouno, A. Nakamura, and M. Yahiro, Phys. Rev. D **93**, 014505 (2016).
[65] C. Pinke and O. Philipsen, *Proc. Sci.*, LATTICE2015, 149 (2016).
[66] F. Cuteri, C. Czaban, O. Philipsen, C. Pinke, and A. Sciarra, Phys. Rev. D **93**, 054507 (2016).
[67] C. Bonati, M. D'Elia, M. Mariti, M. Mesiti, F. Negro, and F. Sanfilippo, Phys. Rev. D **93**, 074504 (2016).
[68] H. Kouno, Y. Sakai, K. Kashiwa, and M. Yahiro, J. Phys. G **36**, 115010 (2009).
[69] Y. Sakai, K. Kashiwa, H. Kouno, M. Matsuzaki, and M. Yahiro, Phys. Rev. D **79**, 096001 (2009).

[70] Y. Sakai, T. Sasaki, H. Kouno, and M. Yahiro, Phys. Rev. D **82**, 076003 (2010); **84**, 091901 (2011).
[71] H. Kouno, M. Kishikawa, T. Sasaki, Y. Sakai, and M. Yahiro, Phys. Rev. D **85**, 016001 (2012).
[72] G. Aarts, S. P. Kumar, and J. Rafferty, J. High Energy Phys. 07 (2010) 056.
[73] J. Rafferty, J. High Energy Phys. 09 (2011) 087.
[74] K. Morita, V. Skokov, B. Friman, and K. Redlich, Phys. Rev. D **84**, 076009 (2011).
[75] K. Kashiwa, T. Hell, and W. Weise, Phys. Rev. D **84**, 056010 (2011).
[76] V. Pagura, D. Gomez Dumm, and N. N. Scoccola, Phys. Lett. B **707**, 76 (2012).
[77] D. Scheffler, M. Buballa, and J. Wambach, Acta Phys. Pol. B Proc. Suppl. **5**, 971 (2012).
[78] K. Kashiwa and R. D. Pisarski, Phys. Rev. D **87**, 096009 (2013).
[79] K. Kashiwa, T. Sasaki, H. Kouno, and M. Yahiro, Phys. Rev. D **87**, 016015 (2013).
[80] P. Weisz, Nucl. Phys. **B212**, 1 (1983).
[81] G. Curci, P. Menotti, and G. Paffuti, Phys. Lett. **130B**, 205 (1983); **135B**, 515(E) (1984).
[82] C. Morningstar and M. J. Peardon, Phys. Rev. D **69**, 054501 (2004).
[83] Y. Aoki, S. Borsanyi, S. Durr, Z. Fodor, S. D. Katz, S. Krieg, and K. K. Szabo, J. High Energy Phys. 06 (2009) 088.
[84] S. Borsanyi, G. Endrodi, Z. Fodor, A. Jakovac, S. D. Katz, S. Krieg, C. Ratti, and K. K. Szabo, J. High Energy Phys. 11 (2010) 077.
[85] S. Borsanyi, Z. Fodor, C. Hoelbling, S. D. Katz, S. Krieg, and K. K. Szabo, Phys. Lett. B **730**, 99 (2014).
[86] C. Bonati, G. Cossu, M. D'Elia, and P. Incardona, Comput. Phys. Commun. **183**, 853 (2012).
[87] C. Bonati, S. Coscetti, M. D'Elia, M. Mesiti, F. Negro, E. Calore, S. F. Schifano, G. Silvi, and R. Tripiccione, Int. J. Mod. Phys. C **28**, 1750063 (2017).